NUMERICAL STUDY OF SUPERSONIC FLOWS AROUND LARGE-ANGLE WEDGES AND CONES

P.I.Chushkin
Computing Centre of the USSR Academy of Sciences,
Moscow, USSR

Abstract

Large-angle wedges and cones with a detached shock wave in a supersonic free-stream are numerically studied using the one-strip method of integral relations in special variables adapted to the flow behaviour near the body apex. Flows about pointed wedges and cones (including those with a concave nose part) at zero angle of attack are computed. Wedges with small bluntness at an angle of attack are also considered. A flow about a wedge-shaped leading edge of an axisymmetric thin-wall ducted body is studied. For pointed wedges some local flow characteristics near the axis are determined. The influence of various parameters is analysed and some effects are found.

I. Introduction

The computation of flows past wedges and cones having the finite length l and the apex semi-angle ω greater than the limiting one is of practical interest. In this case for both pointed and blunted bodies, the detached shock wave formation is mainly determined by the body sides. The mixed subsonic - supersonic flow occurs behind the wave. This problem has not been properly solved yet because of great gradients of gasdynamic functions arising near the body apex.

Flows past wedges and cones at zero angle of attack are calculated easier especially in the case of large bluntness radius. The last case was treated using for example the finite-difference method (1) or the combined finite-difference and characteristics method (2). The flow about a pointed cone transiting into a sphere was studied in (3).

To solve the problem it is advisable to apply the numerical method of integral relations proposed by Dorodnitsyn (4) and developed for the wide class of gasdynamical problems (5). This method was worked out for the supersonic flow around blunted bodies (6,7). The method was used also for pointed wedges and cones in works (8-11) where, however, the nature of the flow close to the body apex was not taken into account and the apex semi-angles were essentially greater than the limiting values and enclosing a narrow range of 10°-15°. Introducing the special coordinates, taking into consideration the singularity at the body front point, the author (12) obtained the solution for sharp wedges and cones with the apex semi-angles going from the limiting values to those exceeding 90° (wedge-shaped and cone-shaped concave noses).

Gasdynamic gradients rise near the body apex especially in the case of a wedge with a small bluntness and a non-zero angle of attack α .* That is why all the earlier calculations of asymmetric two-dimensional flows were restricted to a flat plate (13,14), an asymmetric body

* The case of a cone or an axisymmetrical intake at an angle of attack when the flow is three-dimensional is not considered here.

with a large bluntness [15,16] and a thick ellipse [17]. Recently the author[18] extended his approach [12] to an asymmetric flow past a wedge with a small bluntness.

The problem of supersonic flow about a leading wedge-shaped edge of a ducted axisymmetric body at zero angle of attack is close to the previous problem if an annular zone of mixed flow is formed in front of the inlet lip. Only the simplest case of a ducted body with a flat-faced leading edge was considered earlier [19]. Lately the author solved this problem in the more general case of a wedge-shaped leading edge.

In the one-strip method of integral relations it is possible to improve the linear approximation of any gasdynamic function across the shock layer taking into account its known derivatives on the shock wave and on the body surface [20]. The author [21] applied this approach to predict the stagnation-point velocity gradient and the shock curvature radius on the axis for a flat plate and a disk in a supersonic stream. Now this approach is extended to the case of a wedge at $\alpha = 0$.

The above mentioned author's results concerning the numerical study of supersonic flows about large-angle wedges and cones, is the subject of the present paper.

2. Formulation of problem and method of solution

Taking the more general case of a ducted body, the origin of the Cartesian x, y or the polar r, θ coordinate systems is placed at the apex of the leading edge located at the distance h from the body axis (Fig.1a). When $h = 0$ or $h \to \infty$ we have the cases of a cone or a wedge, respectively. We introduce special orthogonal coordinates ξ, η, connected with the polar coordinates as follows

$$\xi = r^n \sin n(\theta - \omega),$$
$$\eta = r^n \cos n(\theta - \omega),$$
$$n = \pi / 2(\pi - \omega).$$

The line $\xi = \xi_0 > 0$ defines the wedge-shaped body contour with the apex semi-angle ω and the apex curvature radius $R_0 = (1-n)^{-1} \xi_0^{1/n}$. Pointed wedges and cones correspond to $\xi_0 = 0$. The family of such bodies includes wedges and cones ($\omega < \pi/2$), a flat plate and a disk ($\omega = \pi/2$), wedge-shaped and cone-shaped concave noses ($\omega > \pi/2$). The ray $\theta = \pi$ corresponds to the body axis $\eta = 0$.

We shall treat stationary flows of a inviscid nonheat-conducting perfect gas and take the transformed contituity equation and the ξ -momentum equation. In order to improve the computational properties of the solution for bodies with small bluntness and to remove the singularity at the apex for pointed bodies, these equations are multiplied by r^{n-1} in the case of a wedge or a ducted body and by r^{n-2} in the case of a cone. Then these equations can be represented in the divergent form

$$\frac{\partial P_i}{\partial \xi} + \frac{\partial Q_i}{\partial \eta} = G_i \quad , \qquad (1)$$

where P_i, Q_i, G_i ($i = 1,2$) are the functions of ξ, η, the ξ- and η - velocity components u and v, the pressure p and the density ρ, which are considered as dimensionless, being referred to the critical sound velocity and the free-stream density. The Bernoulli integral (instead of the η - momentum equation) and the entropy equation are added to the governing system.

The boundary conditions for the system (1) are specified on the body $\xi = \xi_0$ and on the shock wave $\xi = \xi_1(\eta)$, whe-

re all the quantities are labelled with the subscripts 0 and 1, respectively. On the body $u_0 = 0$ and besides the maximum entropy is assumed to take place here, i.e. the stagnation streamline AB intersects the shock wave at such a point A (Fig.1) where the shock is normal*. Thus at the point A the angle σ between the tangent to the shock and the body axis is $\sigma = \alpha + \pi/2$. The shock wave angle σ is expressed as follows

$$\sigma = \frac{n}{n-1}\tan^{-1}\frac{\xi_1}{\eta} + \tan^{-1}\frac{d\xi_1}{d\eta} + \omega. \qquad (2)$$

The gasdynamic functions on the shock wave are determined from the Rankine-Hugoniot relations in terms of σ, the free-stream Mach number M_∞ and the adiabatic index $\varkappa$ (in the present work $\varkappa = 1.4$).

The numerical solution is obtained by the method of integral relations. Integration of Eq.(1) with respect to ξ from the body to the shock yields the following integral relations

$$\frac{d}{d\eta}\int_{\xi_0}^{\xi_1} Q_i\, d\xi - Q_{i1}\frac{d\xi_1}{d\eta} + P_{i1} - P_{i0} = \int_{\xi_0}^{\xi_1} G_i\, d\xi \quad (i=1,2). \qquad (3)$$

The integrands are approximated linearly using their values on the body and on the shock. Then two ordinary differential equations for the shock wave coordinate ξ_1 and the velocity on the body v_0 are obtained in such a form

$$\frac{d^2\xi_1}{d\eta^2} = \Phi_1, \quad \frac{dv_0}{d\eta} = \frac{\Phi_2}{a_0^2 - v_0^2}, \qquad (4)$$

where at $\eta = 0$ in the axisymmetric case the functions Φ_1, Φ_2 have an indeterminacy which is evaluated using the L'Hospital rule.

The approximating system (4) is integrated numerically from some value $\eta = \eta_A$ corresponding to the shock point A and a priori unknown. There in an asymmetric stream, the initial value of $d\xi_1/d\eta$ is found from Eq.(2) and the condition $\sigma = \alpha + \pi/2$, while the initial value of v_0 is determined using the proposed condition [15] of the zero total mass flow across the line $\eta = \eta_A$. The sonic velocity must be reached at the body corner points C and D (Fig.1), i.e. here $v_0 = 1$ and $v_0 = -1$, respectively. Two these conditions enable to determine at the point A two unknown quantities η_A and ξ_1. They should be found as the result of the solution of this boundary value problem for Eqs.(4) which are repeatedly integrated from $\eta = \eta_A$ until the sonic velocity condition is satisfied at the points C and D. Obviously $\eta_A = 0$ in a symmetric stream ($\alpha = 0$), and then in fact for pointed bodies, the initial value problem for Eqs.(4) takes place.

3. Pointed wedge and cone at zero angle of attack

Flows about pointed wedges and cones with the apex semi-angle ω greater than the limiting ω_* were studied in the case of zero angle of attack. We discuss some results of systematic computations carried out for the body angles within $\omega_* \le \omega \le 180°$ and for the free-stream Mach numbers within $2.5 \le M_\infty \le \infty$.

The shock waves for a family of conical bodies with various ω and $M_\infty = 4$ are shown in Fig.2. When ω tends to its limiting value ω_*, the shock wa-

* The alternative assumption, that the stagnation streamline is straight and normal to the body in the first approximation of the method of integral relations was introduced in [22].

ve at the apex (where the body corners have little effect) approaches the attached conical shock at $\omega = \omega_*$, drawn by the dot-dashed line. The sonic point on the shock wave (marked by the cross) shifts non-monotonically when the angle ω changes. Experimental data [23] for $M_\infty = 4.03$ plotted by the black circles are in the very good agreement with the numerical solution always except the case $\omega = 120°$, where the experimental shock layer is thicker than the calculated one due to intense viscous effect apparently. A similar behaviour of the shock layer, but with larger thickness, also holds for wedges (Fig.3).

The distribution of pressure $\bar{p}_0 = p_0 / p_{0\infty}$, relative to the stagnation pressure, on cones with various ω at $M_\infty = 4$ is presented in Fig. 4 as a function of $\bar{y} = y / y_c$ (y_c is the ordinate of the body corner point C). Near the limiting angle ω_* the $\bar{p}_0$-curves change their shape because the flow turns the conical one. The value of $\bar{p}_0$ at $\omega = \omega_*$ for the attached shock is indicated by the dot-dashed line. As $\omega \to 180°$ then $\bar{p}_0 = 1$ on the whole body surface except the corner point where $\bar{p}_0 = 0.528$. The pressure on wedges (Fig.5) behaves in the same way, but for identical ω (if ω sufficiently exceeds ω_*) it is somewhat lower than on cones.

The drag coefficient C_D for wedges (dashed line) and cones (solid line) is plotted in Fig.6 as the function of ω for various values M_∞. While moving away from $\omega = \omega_*$ the quantity C_D increases and as $\omega \to 180°$ it tends to the value of the pressure coefficient C_p behind the appropriate normal shock. It is interesting that at the considered values of M_∞ the drag coefficient of the cone with the angle ω tending to the limiting one for the flow with the detached shock wave is 11-13% less than for the attached conical shock for the infinite cone with $\omega = \omega_*$. The found effect, remained as ω increases within 10°-20°, is due to the fact that the higher pressure near the cone apex acts on the small area, while the main contribution to C_D is produced by the pressure decrease (in comparison with the constant pressure behind the conical shock for the infinite cone with $\omega = \omega_*$) on the rest part of the body. Recently this effect was confirmed by experiments [23] shown by the black circles in Fig.6.* For wedges the similar effect is not observed in the calculations.

Some local properties of shock waves for wedges (dashed line) and cones (solid line) at $M_\infty = 4$ are described in Fig.7. Here the shock wave detachment distances measured along the axis from the body apex ε and from the body corner cross section ε_c, the curvature radius of shock wave at its apex R_1, the ratio ε / R_1 are plotted versus ω (all these distances are referred to y_c). The ratio ε / R_1 essentially depends on ω (the opposite incorrect conclusion was made in work [9]), it remains finite for $\omega \to \omega_*$ (since both $\varepsilon \to 0$, and $R_1 \to 0$), and tends to infinity as $\omega \to 180°$. The curvature radius has a maximum at some ω.

The change of the ratio ε / R_1 at $\omega \to \omega_*$ in the range $2.5 \leq M_\infty \leq \infty$ is shown in Fig.8. The calcu-

* While this paper was in printing, G. Drougge informed the author that earlier he also found the same effect in the experiment and in the calculation for the transonic flow about cones (Drougge G. The flow around conical tips in the upper transsonic range. Flygtekniska Försöksanstalten FFA, Meddelande No.25, Stockholm, 1948). This publication was not available for the author formerly.

lated limiting values ω_* for wedges (dashed line) and cones (solid line) are compared with the exact theoretical values for infinite bodies (circles), that enables to estimate the numerical solution errors. These errors increase for smaller M_∞ due to a shock layer thickening. However the accuracy of linear approximation is sufficient to predict properly gasdynamic distributions along the body and the shock wave.

4. Wedge with small bluntness at an angle of attack

The computations of flows past wedge-shaped bodies with a small bluntness at an angle of attack were carried out for the following range of parameters: $\omega = 60° - 120°$, $\bar{r}_0 = 0.01 - 0.1$, $M_\infty = 2 - \infty$, $\alpha = 0° - 15°$.

The calculated shock waves for a series of M_∞ at $\alpha = 10°$ are drawn by the solid line in Fig.9 for the blunted wedge $\bar{r}_0 = 0.01$ with the apex semi-angle $\omega = 60°$, having the apex curvature radius $R_0 = 0.0086\, l$ (l is the body length). Here the shock wave for $\alpha = 0°$, $M_\infty = 4$ is also depicted. The sonic points on the shock are marked by the circles, while the initial (A) and the end (B) points of the stagnation streamline are marked by the black circles. The location of the stagnation point B strongly depends on α and almost does not change for various M_∞ within the considered range.

For the same wedge and various α the body surface distributions of the velocity v_0 and the relative pressure $\bar{p}_0$ are plotted versus the relative ordinate $\bar{y}$. An abrupt velocity maximum increasing with the rise of α (and accordingly an abrupt pressure minimum) appears. Here at $\alpha = 15°$ the velocity exceeds the sonic value and thus a local supersonic zone occurs on the body (Fig.10).

The coefficients of tangential force C_t, of normal force C_n and of longitudinal moment C_m as functions of the angle of attack α are presented in Fig.11 for the same wedge $\omega = 60°$. These coefficients are related to the body width $2y_c$, the coefficient of moment C_m, being calculated with respect to the axis passing through the body front point, also includes the length l. When α rises, the pressure on the body windward side increases larger than it drops on the leeward side (see Fig.10), and as a result the tangential force coefficient C_t slightly decreases.

The influence of Mach numbers upon the pressure distribution on the wedge $\omega = 60°$, $\bar{r}_0 = 0.01$ at $\alpha = 10°$ is demonstrated in Fig.12. As M_∞ increases, the pressure drops abruptly on the small bluntness (here at $M_\infty = 7$ the velocity happens to be supersonic) and a considerable difference in pressures on the windward and the leeward sides occurs. The coefficient C_n falls significantly at lower M_∞ due to the more symmetric pressure distribution, while C_t decreases only a little (from 1.55 at $M_\infty = 6$ to 1.45 at $M_\infty = 2$, $\alpha = 10°$). In addition the v_0-curve is drawn to characterize an effect of bluntness radius R_0, which manifests only locally near the body apex. The velocity maximum decreases as R_0 rises, e.g. at $M_\infty = 4$, $\alpha = 10°$ here $v_{0\max} = 0.31$ for $R_0 = 0.064\, l$, but no maximum of v_0 occurs for $R_0 = 0.147\, l$.

Figure 13 shows the influence of the apex semi-angle ω in the case of $M_\infty = 3$, $\alpha = 10°$, $\bar{r}_0 = 0.01$. Here we present the graphs for C_t, the relative ordinates of the points A and B, the shock wave detachment distance ε along the axis $y = 0$, referred

to y_c. It is noticeable that $y_B > y_A$ for $\omega = 120°$.

5. Blunted leading wedge-shaped edge of a ducted body

An annular zone of mixed flow is formed ahead of a blunted leading edge of a ducted axisymmetric body located in a supersonic stream at zero angle of attack, if the relative thickness of the body wall $\delta = 2y_c/(h - y_c)$ is not large, i.e. the radius h (we refer h to y_c) is comparatively great. In this case (see Fig.1a) the mixed flow in the shock layer region, bounded by the characteristic surfaces CE and DF, is formed by the leading edge and does not depend on the gas motion inside the duct. The alternative flow with a single detached shock wave located ahead of the whole ducted body is realized in the other case for large δ or small h. We shall treat the first case of flows about wedge-shaped edges with small bluntness and large apex semi-angles and study the influence of the body geometric parameters and the free-stream Mach number.

The shock waves ahead of the leading edge, having the shape of the blunted wedge $\omega = 60°$, $\xi_0 = 0.01$, $R_0 = 0.0086\,\ell$, are drawn in Fig.14 for a number of M_∞. The shock wave for the same wedge in the two-dimensional flow (as $h \to \infty$) at $\alpha = 0°$, $M_\infty = 4$ is also depicted here by the dashed line. As it is seen shock waves detach from the inner side of the ducted body edge farther than from the outer one. As h increases the stagnation point B shifts to the axis $y = 0$, but its location weakly depends on M_∞.

The distributions of pressure $\bar{P}_0$ and velocity v_0 on the wedge-shaped edges, which have the above considered form, but the different radii h, are presented in Fig.15 for $M_\infty = 4$. When the flow about an edge essentially differs from the two-dimensional one, i.e. h is rather small, an abrupt velocity maximum and a pressure minimum arise on the edge small bluntness.

Now for the same edge we shall analyse the drag coefficient C_D (referred to the area of the annular body cross section) and the coefficient of stream contraction $\sigma = (h + y_A)^2/(h + y_D)^2$. It is shown in Fig.16 how they change with h for a series of M_∞. As it should be expected, when the radius h increases, the drag coefficient rapidly approaches the asymptotic value for the appropriate two-dimensional flow, while the coefficient of stream contraction tends to one. The free-stream Mach number affects C_D appreciably and σ very weakly (in Fig.16 the σ-curve is practically identical for $M_\infty = 2.5 - 6$). Naturally, both coefficients depend on ω.

6. Determination of flow parameters near the axis

In order to improve the accuracy of the one-strip method of integral relations, any integrand in Eqs.(3) can be approximated by the Hermitian third degree polynomials taking into account the values of the appropriate function and its first derivative on the body and on the shock wave. Then

$$\int_{\xi_0}^{\xi_1} Q_i\, d\xi = (Q_{i0} + Q_{i1})\frac{\xi_1 - \xi_0}{2} + \left(\frac{\partial Q_{i0}}{\partial \xi} - \frac{\partial Q_{i1}}{\partial \xi}\right)\frac{(\xi_1 - \xi_0)^2}{12},$$

where the first term concerns the linear approximation. The involved derivatives can be expressed in terms of $d^2\xi_1/d\eta^2$, $dv_0/d\eta$ and the known vorticity on the body and on the shock. As a result instead of Eqs.(4) the other approximating system is derived, namely

$$\frac{d^3\xi_1}{d\eta^3} = \frac{F_1}{\Delta(\sigma)}, \quad \frac{d^2v_0}{d\eta^2} = \frac{F_2}{v_0(a_0^2 - v_0^2)}.$$

We shall consider the case of a flow past a blunted body $\xi = \xi_0$ with the apex semi-angle ω at $\alpha = 0$. Since $v_0 = \Delta(\sigma) = 0$ on the flow axis, the regularity condition provides two equations $F_1 = F_2 = 0$ which have the following form

$$\left(\frac{d\sigma}{d\eta}\right)^2 + a\left(\frac{d\sigma}{d\eta}\right) + b\left(\frac{dv_0}{d\eta}\right) + c = 0,$$
$$\left(\frac{d\sigma}{d\eta}\right)^2 + d\left(\frac{d\sigma}{d\eta}\right) + e\left(\frac{dv_0}{d\eta}\right)^2 + f = 0. \qquad (5)$$

The coefficients in Eqs.(5) are expressed in terms of ω, ξ_0, ξ_1, M_∞, $\varkappa$ and presented in work [21] for $\omega = 90°$, $\xi_0 = 0$.

When a pointed wedge ($\xi_0 = 0$) is considered, the coordinate ξ_1 can be actually eliminated from Eqs.(5) and then the values of $d\sigma/d\eta$ and $dv_0/d\eta$ on the flow axis $\eta = 0$ can be found with the aid of an iterative procedure. In addition, here $\sigma = \pi/2$, $d^2\sigma/d\eta^2 = v_0 = d^2v_0/d\eta^2 = 0$ and consequently using the power series expansions with respect of η, it is possible to determine the flow in the neighbourhood of the axis with acceptable accuracy without integrating the differential equations, but only solving the algebraic equations (5).

The stagnation point velocity gradient dv_0/ds (where s is the arc length along the body $\xi = \xi_0$) is

$$\frac{dv_0}{ds} = n\,\xi_0^{\frac{n-1}{n}}\,\frac{dv_0}{d\eta}.$$

Therefore this gradient is infinite for a pointed wedge, is finite for a flat plate and vanishes for a pointed wedge-shaped concave nose. The curvature radius at the shock wave apex is

$$R_1 = \frac{1}{n}\left(\frac{d\sigma}{d\eta}\right)^{-1}.$$

Referring all the lengths to the shock wave detachment distance ε, we find from Eqs.(5) and plot in Fig.17 the derivative $dv_0/d\eta$ (solid line) and the ratio ε/R_1 (dashed line) versus ω for a series of the free-stream Mach numbers.

References

1. Bohachevsky I.O., Kostoff R.N. AIAA Pap., No.55, 1972.
2. Krasilnikov A.V., Nikulin A.N., Kholodov A.S. Izv. Akad. Nauk SSSR, Mekh. Zhidk. i Gaza, No.2, 179-181 (1975).
3. Ivanova V.N., Radvogin Yu.B. Izv.Akad. Nauk SSSR, Mekh. Zhidk. i Gaza, No.5, 111-115 (1974).
4. Dorodnitsyn A.A. In: Proc. 3rd All-Union Math. Congr. Moscow, 1956. Part III, 447-453, Akad. Nauk SSSR, Moscow, 1958.
5. Belotserkovskii O.M., Chushkin P.I., In: Basic Developments in Fluid Dynamics, vol.1, Acad. Press, New York, 1-126, 1965.
6. Belotserkovskii O.M. Dokl. AN SSSR, 113, No.3, 509-512 (1957).
7. Belotserkovskii O.M., Prikl. Mat. i Mekh., 24, No.3, 511-517 (1960).
8. Bukovshin V.G. Izv. AN SSSR, Mekh. Zhidk. i Gaza, No.2, 83-85 (1969).
9. Rao P.P. AIAA J., 10, No.12, 1573-1581 (1972).
10. Rao P.P. AIAA J., 12, No.4, 421-422 (1974).
11. Grabitz G. Z.angew. Math. und Mech., No.6, Sondern., 200-202 (1968).
12. Chushkin P.I. Zh.Vych. Mat. i Mat. Fiz., 14, No.6, 1600-1605 (1974).
13. Bazzhin A.P. Inzh. Zh., 3, No.2, 222-227 (1963).
14. Archer R.D. AIAA J., 10, No.5, 707-708 (1972).

15. Vaglio-Laurin R. JASS, 29, No.2, 185-206 (1962).
16. Bailey F.R., Rollstin L.R., Iversen J.D. AIAA J., 5, No.10, 1894-1896 (1967).
17. Prosnak W.J. Arch. Mech. Stosow., 16, No.3, 689-708 (1964).
18. Chushkin P.I. Dokl. AN SSSR, 241, No.5 (1978).
19. Betyaev S.K. Izv. Akad. Nauk SSSR, Mekh. Zhidk. i Gaza, No.1, 157-160 (1967).
20. Traugott S.C. JASS, 27, No.5, 361-370 (1960).
21. Chushkin P.I. Chisl. Meth. Mekh. Splosh. Sredy, 7, No.6, 153-160 (1967).
22. Brong E.A., Leigh D.S. AIAA J., 2, No.10, 1852-1853 (1964).
23. Amarantova I.I., Bukovshin V.G., Shustov V.I. Izv. Akad. Nauk SSSR, Mekh. Zhidk. i Gaza, No.2 (1978).

FIGURES

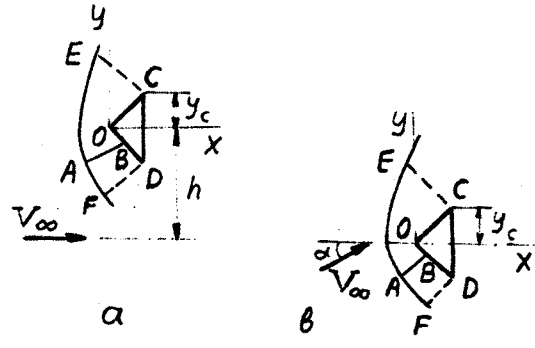

Fig.1. Scheme of flow

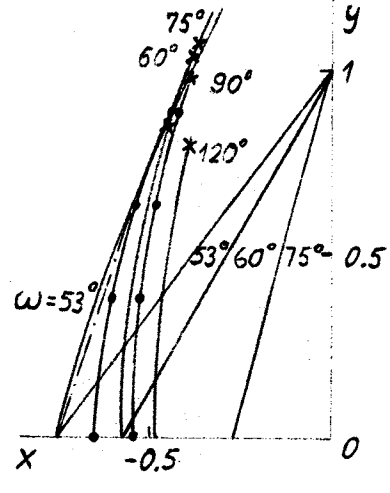

Fig.2. Shock for cones, $M_\infty = 4$.

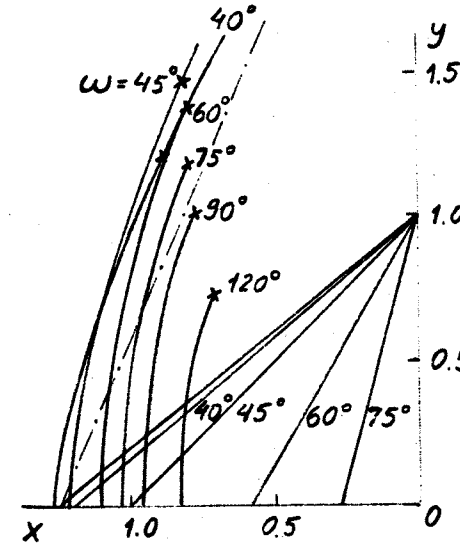

Fig.3. Shock for wedges, $M_\infty = 4$

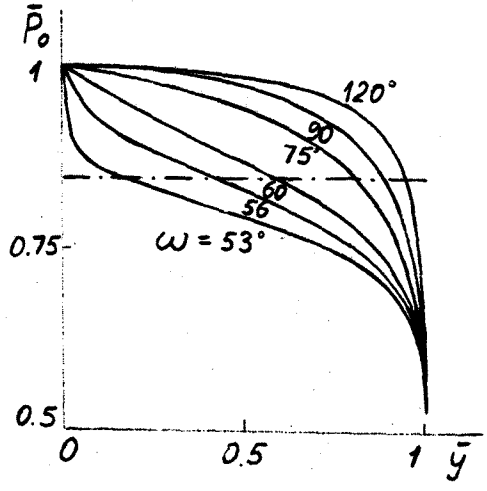

Fig.4. Pressure on cones, $M_\infty = 4$

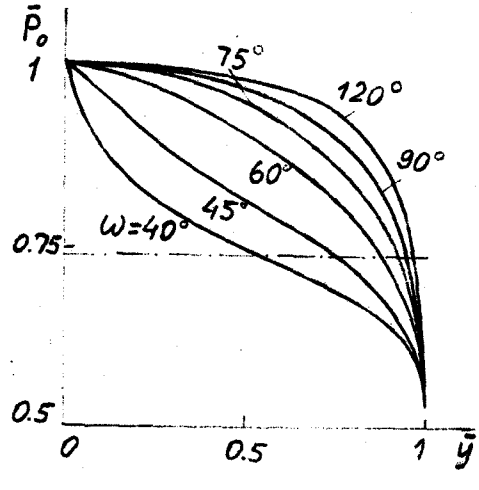

Fig.5. Pressure on wedges, $M_\infty = 4$

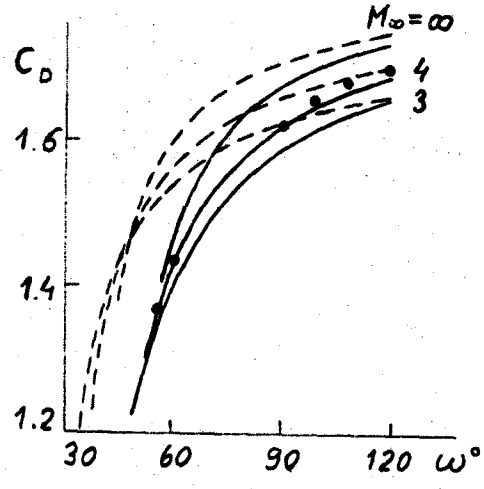

Fig.6. Drag coefficient of cones (solid line) and wedges (dashed line)

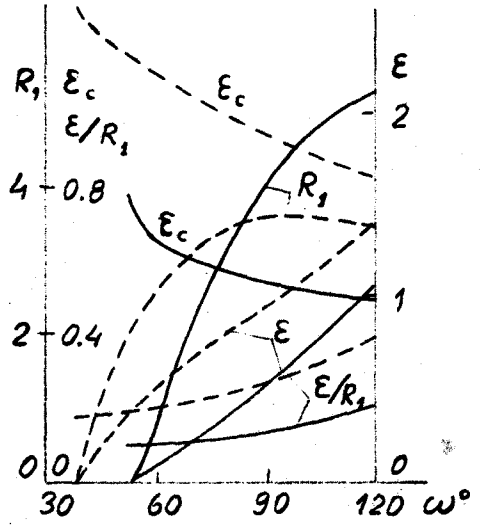

Fig.7. Shock parameters for cones (solid line) and wedges (dashed line), $M_\infty = 4$

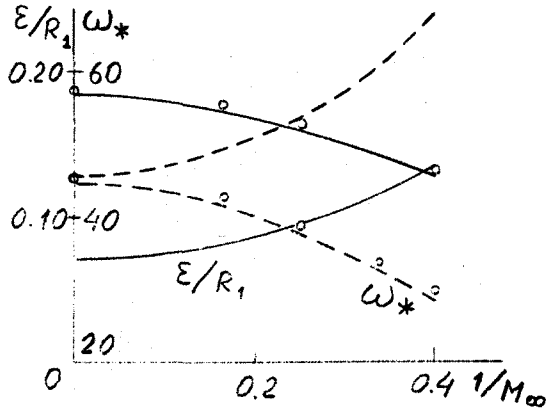

Fig.8. Limiting angle and ratio ε / R_1 for cones (solid line) and wedges (dashed line)

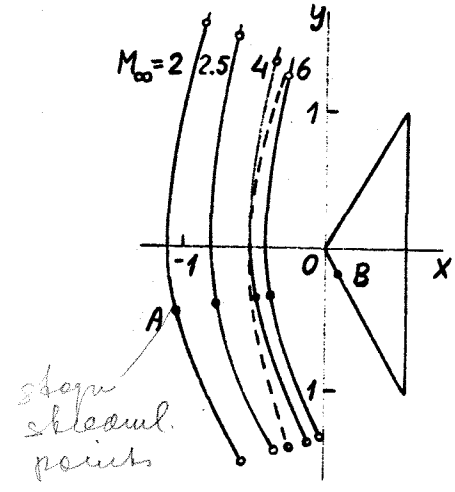

Fig.9. Shock for blunted wedge $\omega = 60°$, $\xi_0 = 0.01$, $\alpha = 10°$.

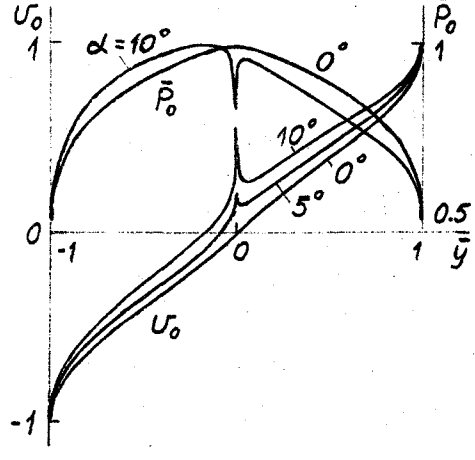

Fig.10. Pressure and velocity on wedge $\omega = 60°$, $\xi_0 = 0.01$, $\alpha = 10°$

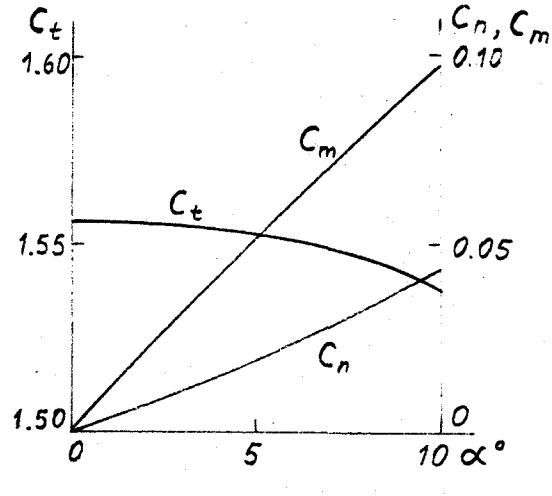

Fig.11. Aerodynamic coefficients of wedge $\omega = 60°$, $\xi_0 = 0.01$, $M_\infty = 4$

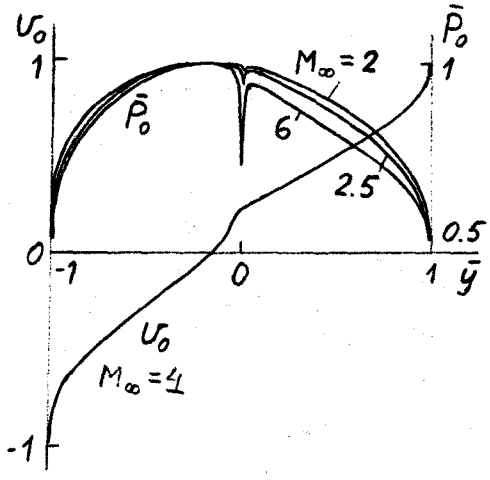

Fig.12. Pressure on wedge $\omega = 60°$, $\xi_0 = 0.01$, $\alpha = 10°$ and velocity $\xi_0 = 0.1$, $\alpha = 10°$

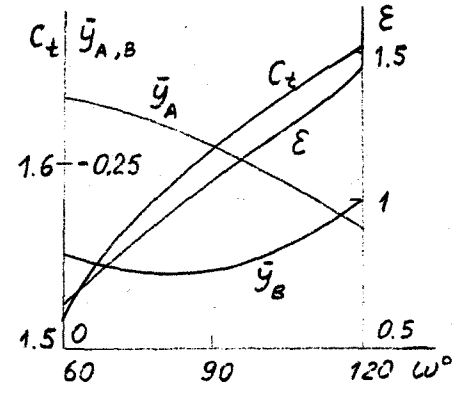

Fig.13. Flow parameters for wedges $\xi_0 = 0.01$, $\alpha = 10°$, $M_\infty = 3$

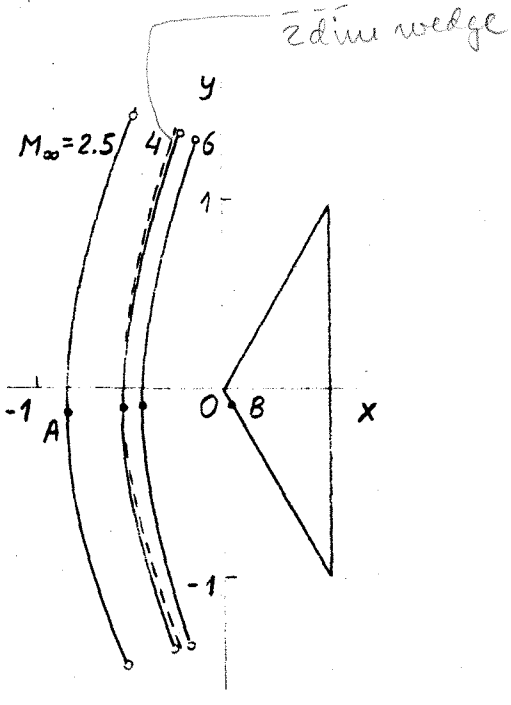

Fig.14. Shock for blunted edge of duct $\omega = 60°$, $\xi_0 = 0.01$, $h = 6$ $\alpha = 0°$

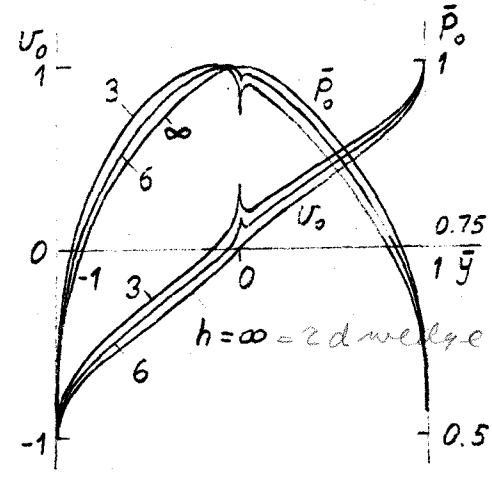

Fig.15. Pressure and velocity on duct edges $\omega = 60°$, $\xi_0 = 0.01$, $M_\infty = 4$

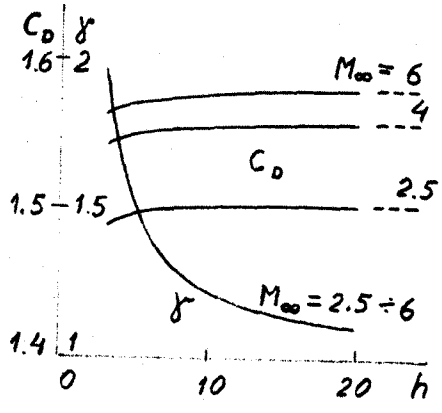

Fig.16. Drag and stream contraction coefficients for duct edges $\omega = 60^\circ$, $\bar{x}_0 = 0.01$, $M_\infty = 4$

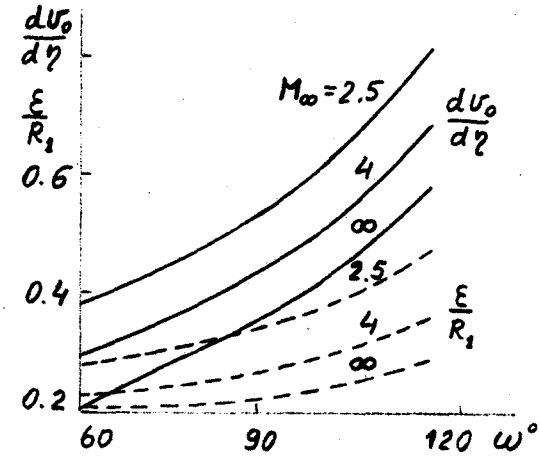

Fig.17. Velocity derivative and ratio ε/R_1 on axis for wedges